



# Experimental investigation of the effects of floating wind turbine motion on a downstream turbine performance and loads

Alessandro Fontanella<sup>1</sup>, Stefano Cioni<sup>2</sup>, Francesco Papi<sup>2</sup>, Sara Muggiasca<sup>1</sup>, Alessandro Bianchini<sup>2</sup>, and Marco Belloli<sup>1</sup>

<sup>1</sup>Department of Mechanical Engineering, Politecnico di Milano, via La Masa 1, 20156 Milano, Italy.

<sup>2</sup>Department of Industrial Engineering, Università degli Studi di Firenze, Via di Santa Marta 3, 50139 Firenze, Italy.

**Correspondence:** Alessandro Fontanella (alessandro.fontanella@polimi.it)

**Abstract.** This study investigates how the motion of a floating wind turbine affects the aerodynamic performance and dynamic loading of a downstream turbine operating in its wake. Wind tunnel experiments were conducted using a two-turbine setup, where the upstream turbine was subjected to controlled platform motions (both sinusoidal and wave driven) while the downstream turbine remained fixed and was tested in multiple relative positions. Results show that large-amplitude, low-frequency, sinusoidal motions of the upstream turbine, especially in crosswind and yaw directions, can increase the power output of the downstream turbine under low-turbulence conditions and at short turbine spacing (3-5 rotor diameters). The largest relative power gain reached 26% over the fixed case, although absolute gains remained moderate. The gains obtained under idealized sinusoidal motions were replicated in cases with realistic-wave-driven motions when wind and waves were aligned, but not when wind-wave misalignment introduced crosswind movements of the upstream wind turbine. In parallel, motion of the upstream turbine increased the dynamic loading on the waked turbine. These effects varied with turbine spacing and alignment, and were more pronounced in sinusoidal motion cases. Still, similar mechanisms were observed under wave-induced motion. Overall, these findings underscore that platform-induced wake dynamics are not a secondary effect, but a key driver that must be considered in the design and operation of floating wind farms.

## 1 Introduction

The deployment of floating offshore wind farms is a key strategy to harness wind energy in deep-water regions where fixed-bottom turbines are not feasible. While the floating wind technology enables access to abundant yet untapped wind resources, it also introduces additional complexities, especially regarding system dynamics due to the large motions of platforms and their influence on the wind turbine aerodynamic response. In particular, the aerodynamic interactions between wind turbines through wakes, which is already a critical factor in bottom-fixed wind farms, become even more complex in floating wind farms, as the aforementioned large platform motions typical of this technology may lead to more unsteady and irregular wake flows. These wake effects can lead to substantial power losses, increased fatigue loads, and control challenges at the turbine and plant levels. Despite their importance they remain poorly understood in the context of floating wind farms (Meyers et al., 2022) and one reason for the limited understanding of aerodynamic interactions in floating wind farms is the lack of wake and



performance data from operational plants. To date, only a few floating wind farms have been constructed, each comprising a  
25 small number of turbines (Chitteth Ramachandran et al., 2022).

Most available studies focus on the wake behavior of individual floating turbines and do not address how turbines interact  
through wakes within a full wind farm. A recent study by Angelou et al. (2023) examined the far wake of a 6 MW floating wind  
turbine in the Hywind Scotland offshore wind farm, the world's first floating wind farm, using LiDAR measurements. Its find-  
ings indicate that the wakes of floating turbines, for small-amplitude dynamic motions of the platform, exhibit time-averaged  
30 characteristics similar to those of fixed-bottom turbines. Under these conditions, atmospheric turbulence was identified as the  
dominant mechanism for wake recovery, with platform motion having a negligible effect. However, the investigation focused  
on conditions in which the turbine operated outside the wake of upstream units, and therefore did not address the impact of  
upstream wakes on turbine performance within the array.

The impact of large platform motions on the wake behavior of floating wind turbines has been instead extensively inves-  
35 tigated through wind tunnel experiments, which offer controlled and repeatable conditions ideal for isolating aerodynamic  
phenomena. Most of these studies have employed model-scale wind turbines subjected to unidirectional sinusoidal motions of  
large amplitude and low frequency, typically in low-turbulence inflow.

The experiment of Bayati et al. (2017a) analyzed the effect of surge motion on the near wake of a 1:75 scale model of the  
DTU 10 MW wind turbine (Bak et al., 2013), demonstrating that platform motion introduces wind speed fluctuations in the  
40 wake. Building on this, Fontanella et al. (2022b) explored additional surge motion conditions and showed how motion affects  
the formation and evolution of tip vortices near the rotor. In a later study, Fontanella et al. (2022a) investigated the wake of a  
1:100 scale model of the IEA 15 MW reference turbine (Gaertner et al., 2020) under platform motions in along-wind and cross-  
wind directions. The results indicated that all motion types induced velocity fluctuations in the wake, although mean velocity  
in the near wake was slightly reduced compared to the fixed-turbine case. Messmer et al. (2024a) further examined wake  
45 behavior under harmonic surge and sway motions in laminar inflow conditions. The study found that sway motion enhances  
lateral meandering, while surge motion induces wake pulsation; both contribute to improved mixing and recovery of the far  
wake. In a follow-up study, Messmer et al. (2024b) assessed the effect of surge motion under inflow turbulence intensities up  
to 3%, showing that increased turbulence significantly diminishes the influence of platform motion on the far wake recovery.  
Bossuyt et al. (2023) investigated a 1:400 scale floating wind farm with twelve turbines in a wind–water tunnel under a sheared  
50 inflow with 10% turbulence intensity. Despite the challenges of simultaneously scaling aerodynamics and hydrodynamics, the  
study revealed clear differences in wake recovery linked to the periodic rotor motions. Wave-induced yaw and pitch led to  
synchronized vertical wake oscillations that enhanced recovery but also increased turbulence levels, potentially affecting the  
unsteady loading on downstream turbines.

Taken together, these experiments consistently demonstrate that large rotor motions influence wake development, generating  
55 flow structures with the same periodicity as the platform motion. These dynamic features, primarily seen as pulsations in  
velocity and increased lateral meandering, are absent in wakes of bottom-fixed turbines. Under nearly laminar conditions,  
such wake dynamics can enhance recovery, but their effect becomes negligible as inflow turbulence increases. At low but



realistic turbulence intensities, platform motions still generate coherent periodic structures, but they do not lead to substantial improvements in wake recovery.

60 The limited availability of experimental data has led to diverse modeling approaches for floating wind farms, often yielding scattered results. Carmo et al. (2024) used FAST.Farm, which neglects dynamic wake effects due to platform motion, modeling only the wake vertical deflection due to average rotor inclination. This simplification was deemed acceptable under typical turbulence conditions, where wake pulsing effects are expected to be minimal. In contrast, Ramos-García et al. (2022) used a vortex-multibody solver to show that platform motions in an upstream turbine enhance wake breakdown, increasing power and  
65 thrust in downstream turbines and that this effect diminishes with higher inflow turbulence. Simulations with prescribed surge and pitch motions confirmed that platform dynamics significantly affect wake behavior and downstream loading, especially deeper in the array where resonant interactions may occur.

A number of numerical studies using computational fluid dynamics (CFD) have investigated wake behavior in floating wind turbines, often focusing on isolated machines (Micallef and Rezaeiha, 2021). Moving toward farm-scale interactions,  
70 Arabgolarcheh et al. (2023) used unsteady Reynolds-averaged Navier–Stokes (URANS) simulations to examine the effect of prescribed surge motion on two aligned floating wind turbines. While the mean thrust and power output showed little difference between fixed and surging upstream rotors, the motion generated periodic wake structures that increased dynamic loading on the downstream turbine. Similarly, Li et al. (2025) employed large eddy simulation (LES) to study wake interactions between two surging turbines and found that, under laminar inflow, the downstream power increased significantly. However,  
75 this gain became negligible under more realistic turbulence levels. Additional insight into the physical mechanisms governing this behavior has recently been provided by Pagamonci et al. (2025), who conducted LES-based CFD simulations on the same wind tunnel-scale turbine used in the present study. Their results show that under turbulent inflow conditions, tip vortex breakdown occurs much closer to the rotor compared to laminar inflow, leading to markedly different wake development than what is predicted under idealized flow conditions.

80 Although CFD studies provide valuable insights into wake dynamics and turbine interactions, their results often vary due to differences in turbulence modeling, inflow conditions, and domain size. This variability limits their reliability in predicting wake effects in realistic floating farm configurations. This motivates the need for controlled experimental data, which can serve both to understand key physical mechanisms and to validate or calibrate numerical tools.

This study investigates, through wind tunnel experiments, how wakes generated by floating wind turbines affect the dynamic  
85 loading and power output of a downstream turbine operating in their wake. Specifically, it seeks to address two key research questions:

1. Do the unsteady flow disturbances induced by platform motion propagate downstream and influence the load response of a waked turbine?
2. Can a turbine operating in the wake of a moving upstream rotor extract more power than one operating behind a bottom-  
90 fixed turbine?



The experiment and its results are presented in the following sections. Section 2 describes the methodology of the study, including the experimental setup, the operating conditions of the wind turbines, and the platform motions. Section 3 presents and analyzes experimental results. In Section 4, these results are discussed with the aim of evaluating their relevance and applicability to the design and operation of floating wind farms. This discussion also considers the limitations and simplifications inherent to the experimental setup. Finally, Section 5 summarizes the main findings of the study and outlines the conclusions.

## 2 Methodology

The experimental campaign was conducted in the atmospheric-boundary layer test section of Politecnico di Milano wind tunnel, which is 13.84 m wide by 3.84 m high by 35 m long and used two wind turbines (WT) that are 1:75 scale models of the DTU 10 MW reference wind turbine (Bak et al., 2013). In the experiment, the flow speed was scaled by a factor 1:3 compared to a full-scale environment. The time scaling in the experiment was determined by the geometric and velocity scales, resulting in a time scale ratio of 1:25. Consequently, the wind farm response in the experiment occurred 25 times faster than at full scale.

In the experiment, only the upstream turbine was subjected to platform motions representative of a floating wind turbine, while the downstream turbine was fixed at the tower base. This approach avoids introducing additional variables that could make it more difficult to identify the specific influence of the upstream turbine dynamics on the downstream turbine response. Similar methodologies have been employed in previous wind tunnel studies on wake interactions, particularly in active wake control research, where only the most upstream turbine is dynamically actuated, and downstream turbines are operated with fixed settings (Van Der Hoek et al., 2024; Van Der Hoek et al., 2024). Once the effects of upstream rotor motion are well understood, the analysis can be extended to more realistic scenarios that also include the motion of the downstream turbine.

The experiment with two turbines followed the one of Fontanella et al. (2024), that was performed in the same wind tunnel using the same wind turbine and robotic platform and measured the wake of the upstream wind turbine at the downstream locations where WT2 was placed in the current experiment. Hence, the inflow caused by the wake of the upstream turbine on the downstream turbine is precisely known because it has been already characterized.

### 2.1 Experimental setup

The experimental setup is shown in Fig. 1. The upstream wind turbine (WT1) was mounted on a six-degrees-of-freedom robotic platform that mimics the rigid-body motions of floating foundations. The downstream wind turbine (WT2) was mounted on a rigid support structure connecting the tower base to the wind tunnel floor.

The two wind turbines are identical. Their main geometric parameters are summarized in Table 1. The rotors of the wind turbines have a diameter ( $D$ ) of 2.38 m and were designed to replicate at small scale the normal load distribution of the DTU 10 MW blade and the resulting thrust force (Bayati et al., 2017b). The shaft of the wind turbines had a tilt of  $5^\circ$ , matching the full-scale version of the DTU 10 MW. During wind tunnel tests, the towers of the two wind turbines were tilted at a negative angle of  $5^\circ$  to ensure the rotors were vertical to the wind tunnel floor. This simplification was intended to limit the analysis to axial thrust and torque in scenarios without prescribed platform motion and with the turbine operating in undisturbed flow.

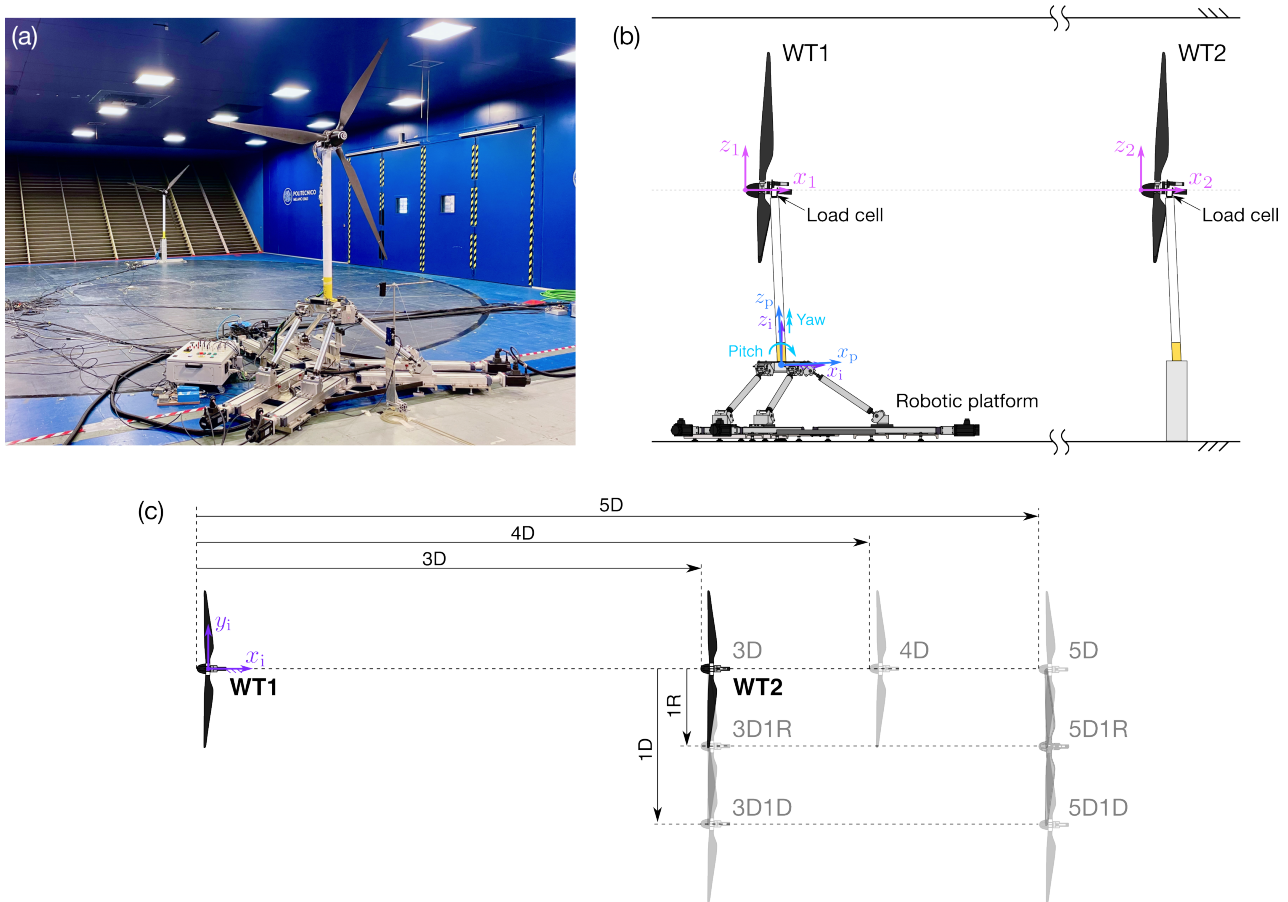


**Figure 1.** Experimental setup. (a): the two wind turbines in the wind tunnel, positioned at a distance of five rotor diameters ( $D$ ), with a lateral offset of one radius ( $R$ ). (b): schematic representation of the experimental setup with the coordinate systems. (c): wind farm configurations that were tested.

During the experiment, the position of WT2 relative to WT1 was varied to investigate how downstream distance and cross-wind offset influence the response of the downstream turbine, as illustrated in Fig. 1. WT2 was placed at downstream distances of  $3D$ ,  $4D$ , and  $5D$  along the same line as WT1. The maximum spacing was limited by the dimensions of the wind tunnel test section, which did not permit to place the downstream turbine beyond  $5D$ . While these spacings are shorter than those typically used in commercial wind farms, generally ranging from 6 to 10 rotor diameters (Stevens et al., 2017), they are particularly relevant for experimental investigation, as the dynamic wake behaviors induced by platform motion remain well-defined at these distances and can significantly affect the performance and loading of downstream turbines (Fontanella et al., 2024; Firpo et al., 2024). Studying these effects at short spacing helps isolate and amplify the impact of wake–motion interactions, providing insight into its fundamental mechanisms before turbulence and wake recovery dominate at larger spacings.



**Table 1.** Geometry of the wind turbines used in the experiment.

Parameter	Unit	Value
Rotor diameter ( $D$ )	m	2.381
Blade length	m	1.102
Hub diameter	m	0.178
Hub height	m	2.190
Rotor overhang	m	0.139
Shaft tilt angle	°	5
Tower-to-shaft distance	m	0.064
Tower length	m	1.400
Tower diameter	m	0.075
Tower base offset from ground	m	0.730

For the  $3D$  and  $5D$  configurations, WT2 was also shifted laterally in the negative  $y$ -direction by either  $1R$  or  $1D$ , where  $R$  is the rotor radius. When offset by  $1R$ , approximately half of WT2 rotor is immersed in the wake of WT1; with a  $1D$  offset, most of the rotor operates in free-stream flow, with only a small portion affected by the wake.

135 The WT1 platform position was measured using Wenglor PNBC107 laser transducers. The rotor forces of both wind turbines were measured using six-component ATI Mini45 force transducers (SI-580-20 calibration), mounted at the top of each tower. For WT1, the recorded loads include not only the aerodynamic forces generated by the rotor but also the inertial and gravitational loads of the rotor–nacelle assembly due to its motion. These non-aerodynamic contributions were removed following the method described by Fontanella et al. (2022a), allowing isolation of the pure aerodynamic loads. All aerodynamic forces  
140 are expressed in the respective hub reference frames:  $x_1 - y_1 - z_1$  for WT1 and  $x_2 - y_2 - z_2$  for WT2. The resulting signals contain approximately 100 full cycles of platform motion, ensuring a robust characterization of the quasi-periodic aerodynamic response.

Complementary measurements of the streamwise velocity in the turbine wake were performed in a prior experimental campaign using a single hot-wire anemometer capable of measuring both mean and fluctuating components of one-dimensional  
145 flow (Fontanella et al., 2024). The probe was mounted on an automated traversing system, enabling measurements in the crosswind ( $y_i - z_i$ ) plane. Velocity data were collected along lines at  $x_i = 3D, 4D, 5D$  downstream of the rotor, centered horizontally on the hub (along the  $y_i$ -axis), at 35 evenly spaced points. Spatial velocity fields were reconstructed by phase-aligning the measurements with the platform motion signal.

## 2.2 Wind turbine operating settings

150 All the tests were carried out for a constant wind speed ( $U$ ) of  $3.9 \text{ ms}^{-1}$ , measured by a Pitot tube positioned  $3.13D$  ahead of the wind turbine on the hub axis. The free-stream flow was approximately uniform across the wind tunnel test section,



as demonstrated in a previous study (Fontanella et al., 2024). The mean velocity over the WT1 rotor area varied by 5% compared to the hub mean velocity, and the average turbulence intensity across the rotor disk was 1.5%. Large-eddy simulations of Pagamonci et al. (2025) have shown that this relatively low free-stream turbulence has a noticeable influence on wake development.

Another Pitot system was placed laterally to WT1 at  $x_i = 0.8D$ ,  $y_i = 2.1D$ , and  $z_i = 1.3D$  to measure the wind speed influenced by blockage effects induced by the WT1 rotor, recording a wind speed of  $4.2 \text{ ms}^{-1}$ . The increase in wind speed due to wind tunnel blockage is sufficiently small, and multi-fidelity simulations by Bergua et al. (2023) on the wind turbine used in this study showed that blockage does not significantly alter its aerodynamic behavior. The effect can be accurately introduced in simulations by applying a corrected inflow velocity that reflects the value measured by the lateral Pitot system.

During testing, the air density ( $\rho$ ) was  $1.187 \text{ kgm}^{-3}$ .

WT1 had a fixed rotor speed of 240 rpm and a collective blade pitch set to the optimal value of  $0^\circ$ . The turbine operated near its rated condition, where it generated maximum thrust and thus produced a significant wake deficit.

The uniformity of the inflow generated by the wind tunnel across the region occupied by the wind farm was verified by measuring the loads on WT2 positioned at  $5D$  downstream, under free-stream conditions with WT1 removed from the test chamber. This verification also ensured that WT2, when placed in the most downwind position, was not influenced by boundary effects near the end of the test section. Measurements were conducted at two wind speeds:  $3.9 \text{ ms}^{-1}$  and  $2.4 \text{ ms}^{-1}$ . The latter corresponds to the average wind speed over the rotor plane in the  $5D$  full-wake condition, as estimated from the wake measurements reported by Fontanella et al. (2024). At  $2.4 \text{ ms}^{-1}$ , the rotor speed was set to 150 rpm to maintain the optimal tip speed ratio of 7.5.

The energy available to WT2 when operating in non-free-stream conditions is reduced due to wake losses, which depend on its position relative to the upstream turbine. When outside of free-stream conditions, WT2 operated in a non-uniform wind field due to partial or total immersion in the wake of WT1, depending on its position. The operating conditions of WT2 were defined in terms of rotor-effective wind speed ( $U_{RE}$ ), estimated from rotor thrust measurements at each location with fixed WT1. The blade pitch of WT2 was fixed at  $0^\circ$ , as for WT1, and was not adjusted based on the rotor-effective wind speed in order to avoid added complexity and to better isolate the effects of the wake on aerodynamic loading. WT2 rotor speed was adjusted to the values specified in Table 2 to attain the optimal tip speed ratio calculated based on  $U_{RE}$  except for the 3D1D and 5D1D configurations, where rotor speed was set to maintain the same thrust force as in the free-stream condition, despite  $U_{RE}$  being higher than the free-stream wind speed. In the 5D1D configuration, the  $U_{RE}$  for WT2 is higher than both the free-stream wind speed and the wind speed measured by the lateral Pitot system, which accounts for the blockage effect of WT1. The additional increase in velocity observed at WT2 is attributed to the local blockage caused by the WT2 rotor itself. The rotor speed of WT2 in situations involving the movement of WT1 remained consistent with that of the fixed case.



**Table 2.** Rotor effective wind speed ( $U_{RE}$ ) and rotor speed of the downstream wind turbine in the different wind farm configurations tested in the experiment.

Configuration	$U_{RE}$ [m/s]	Rotor speed [rpm]
3D	2.1	130
3D1R	3.3	190
3D1D	4.5	220
4D	2.3	140
5D	2.4	150
5D1R	3.3	190
5D1D	4.5	230

### 2.3 Platform motion scenarios

The experiment included both unidirectional sinusoidal motions and realistic platform motions representative of a 10 MW floating wind turbine subjected to irregular wave excitation.

Platform motions were defined using the inertial reference frame ( $x_i - y_i - z_i$ ) and the platform reference frame ( $x_p - y_p - z_p$ ) that are depicted in Fig. 1b. The platform reference frame is fixed to the robotic platform and moves with the turbine; it has the origin  $O_p$  in correspondence of the tower base, on the tower centerline.  $z_p$  points along the tower axis,  $x_p$  points in the downwind direction when the platform is fixed and  $y_p$  forms a right-hand backhoe with  $x_p$  and  $z_p$ . The origin of the inertial reference frame  $O_i$  is at a vertical distance of 0.73 m from the ground. When the wind turbine is in the fixed position  $O_p$  is coincident with  $O_i$ .

#### 2.3.1 Sinusoidal motion

The system was studied under sinusoidal motion of different frequencies and amplitudes. The platform displacement, whether it involved a translation or a rotation, was defined as:

$$d(t) = a_m \cdot \sin(2\pi f_m t), \quad (1)$$

where  $a_m$  is the amplitude of platform motion and  $f_m$  the motion frequency.

In research concerning the unsteady aerodynamics of floating wind turbines (Fontanella et al., 2021; Messmer et al., 2024a), frequencies are typically expressed in a non-dimensional form using the rotor reduced frequency ( $f_r$ ), which is equivalent to a Strouhal number and is defined as:

$$f_r = \frac{f_m D}{U}. \quad (2)$$

The surge motion corresponded to the translation of  $O_p$  along  $x_i$ , pitch was the rotation around the  $y_i$  axis, and yaw the rotation around the  $z_i$  axis; the rotations are illustrated in Fig. 1b. Furthermore, the experiment explored platform movements



at different angles relative to the wind direction. The surge–sway motion at an angle  $\gamma$  refers to the translation  $d$  along an axis that forms an angle  $\gamma$  with the  $x_i$ -axis and consequently with the wind. This motion has a component along the surge direction  
205  $d_x(t) = d(t) \cdot \cos \gamma$  and a component in the cross-wind (sway) direction  $d_y(t) = d(t) \cdot \sin \gamma$ . During the test values of  $\gamma$  of  $15^\circ$ ,  $30^\circ$ ,  $45^\circ$ , and  $90^\circ$  were investigated.

Surge and pitch motions cause along-wind movement of the nacelle and result in an apparent wind speed over the rotor that is:

$$u_a(t) = U - \dot{d}_{\text{hub},x}(t), \quad (3)$$

210 where  $\dot{d}_{\text{hub},x} = \dot{d}$  in case of surge motion,  $\dot{d}_{\text{hub},x} = \dot{d} \cos \gamma$  in case of surge-sway motion, and  $\dot{d}_{\text{hub},x} = \dot{d} \cdot r_{\text{hub}}$  in case of pitch motion, where  $r_{\text{hub}}$  is the distance between the rotor apex and the platform rotation point  $O_i$ .  $u_a$  has oscillations of amplitude  $\Delta u = 2\pi f_m a_m$  in case of surge motion,  $\Delta u = 2\pi f_m a_m \cdot \cos \gamma$  in case of surge–sway motion, and  $\Delta u = 2\pi f_m a_m \cdot r_{\text{hub}}$  in case of pitch motion. During yaw motion, because the yaw amplitude is small, the apparent velocity is mainly in the  $x_i$  direction. This velocity has a gradient across the rotor span, it reaches the maximum in amplitude at the rotor edge and is zero in  
215 correspondence of the hub. The velocity profile is:

$$u_a(t, p_y) = U - \dot{d}(t) \cdot p_y, \quad (4)$$

where  $p_y$  is the distance, with sign, on the  $y_p$ -axis from the rotor apex. The apparent wind velocity has oscillations with an amplitude of  $\Delta u(p_y) = 2\pi f_m a_m \cdot p_y$ .

The sinusoidal motion conditions were characterized in terms of reduced frequency and amplitude. The selected amplitudes  
220 and frequencies were based on those used the previous wind tunnel experiment of Fontanella et al. (2024) that characterized the wake behavior. The selected conditions were known to cause significant dynamic variations in the wake and were consequently expected to produce a substantial aerodynamic excitation of the downstream turbine. The frequencies correspond to reduced frequency values representative of full-scale floating wind turbine dynamics. Specifically,  $f_r = 0.3$  and  $f_r = 0.6$  correspond to full-scale frequencies of 0.02 Hz and 0.04 Hz, respectively, which are typical of rigid-body modes in 10 MW floating turbines.  
225 In contrast,  $f_r = 1.2$  corresponds to a full-scale frequency of 0.08 Hz (with a period of 12.5 s), representative of platform motions at wave frequency.

The amplitudes of surge and pitch motions caused an apparent wind speed variation, expressed as a ratio of apparent wind to undisturbed wind speed ( $\Delta u/U$ ), of approximately 5% at all reduced frequency values considered in the experiment. In surge–sway motion, the displacement amplitude  $d$  was the same as in pure surge, but the variation in apparent wind speed  
230 decreased as the angle between the motion direction and the wind ( $\gamma$ ) increased. For yaw motion, an amplitude of  $2^\circ$  was selected, to investigate wake development under large dynamic yaw rotations, representative of those that may occur in real operating conditions under severe sea states. When combined with reduced frequencies of 0.3, 0.6, and 1.2, this yaw motion amplitude resulted in apparent wind speed variations at the rotor edge of approximately 3%, 7%, and 13%, respectively.



### 2.3.2 Irregular waves

235 Following the analysis of cases with sinusoidal motions, the experiment was extended to include motions similar to those induced by irregular waves propagating from different directions, in order to assess whether the observations from the simplified cases remained valid under more realistic conditions.

In these tests, unlike the sinusoidal cases, the wind turbine motion is not defined by simple parametric inputs but is derived from the dynamic response of a realistic floating wind turbine. Specifically, we considered the SOFTWIND system, consisting of the DTU 10 MW wind turbine mounted on a spar-buoy platform (Arnal, 2020; Behrens de Luna et al., 2024; Papi et al., 2024). Table 3 reports the frequencies of the rigid-body motion modes of the SOFTWIND floating wind turbine. At these frequencies, the motion of the floating wind turbine exhibits large amplitudes due to the dynamic amplification of the wind and waves forcing.

**Table 3.** Frequencies of the rigid-body motion modes of the SOFTWIND floating wind turbine.

Mode	Frequency (full scale) [Hz]	Frequency (model scale) [Hz]
Surge and sway	0.008	0.208
Roll and pitch	0.031	0.780
Yaw	0.077	1.925

Motion time series were generated before the experiment using OpenFAST. The waves in the simulation had a full-scale significant height of 5 m and a peak period of 12 s corresponding to a model-scale significant height of 0.067 m and a peak period of 0.48 s. The same waves were applied at heading angles of 0° and 30° relative to the wind direction. The simulations were carried out with a uniform wind field with a full-scale wind speed of 12 ms<sup>-1</sup> and turbulence intensity of 1.5%, fixed rotor speed and blade pitch, matching the conditions of the experiment. The resulting time series of platform motions in six directions were downscaled and employed to prescribe the motion of WT1 utilizing the robotic platform.

250 The time series of platform motions induced by irregular waves are shown in Fig. 2 and the corresponding spectra in Fig. 3. When waves are aligned with the wind direction (0°), the platform response is dominated by surge and pitch, with minimal motion in the other degrees of freedom. In contrast, waves at 30° also excite significant sway, roll, and yaw movements. Figure 2 shows that the frequency and amplitude of the platform motions of the SOFTWIND driven by the selected wave conditions are similar to those in the sinusoidal motion cases. Specifically, sinusoidal surge–sway and yaw motions represent 255 movements in the sway and yaw directions caused by waves with a 30° heading.

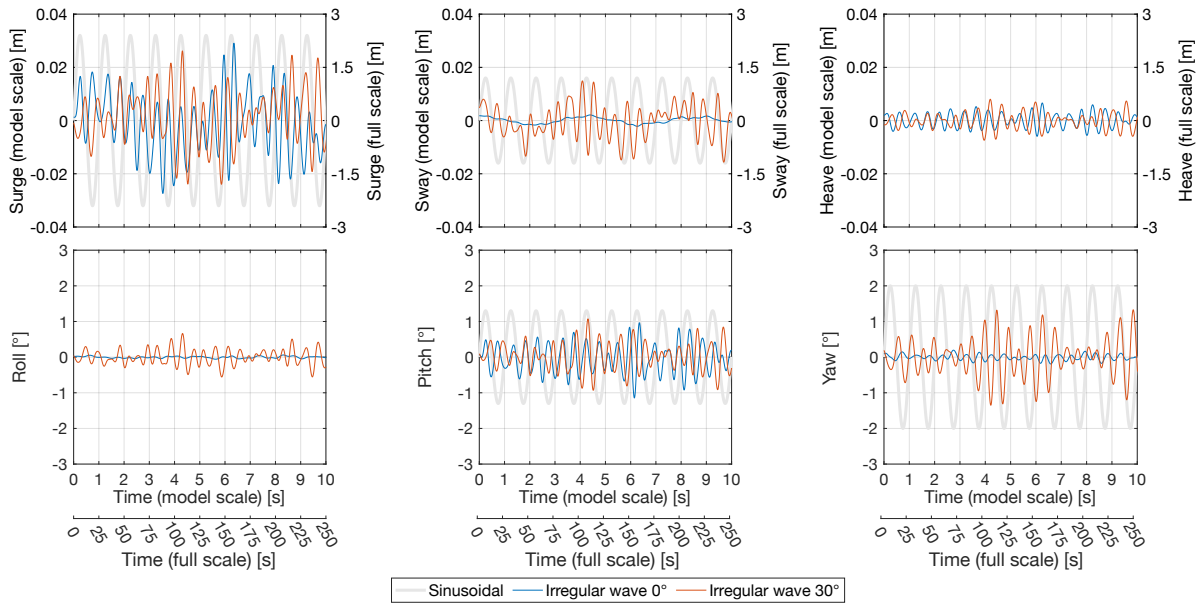


**Figure 2.** The time series of wave-induced motions examined in the experiment are compared with sinusoidal motions of  $f_r = 0.6$ . The wave-induced motions correspond to the SOFTWIND 10 MW floating wind turbine subjected to irregular waves with a significant height of 5 m and a peak period of 12 s (full scale).

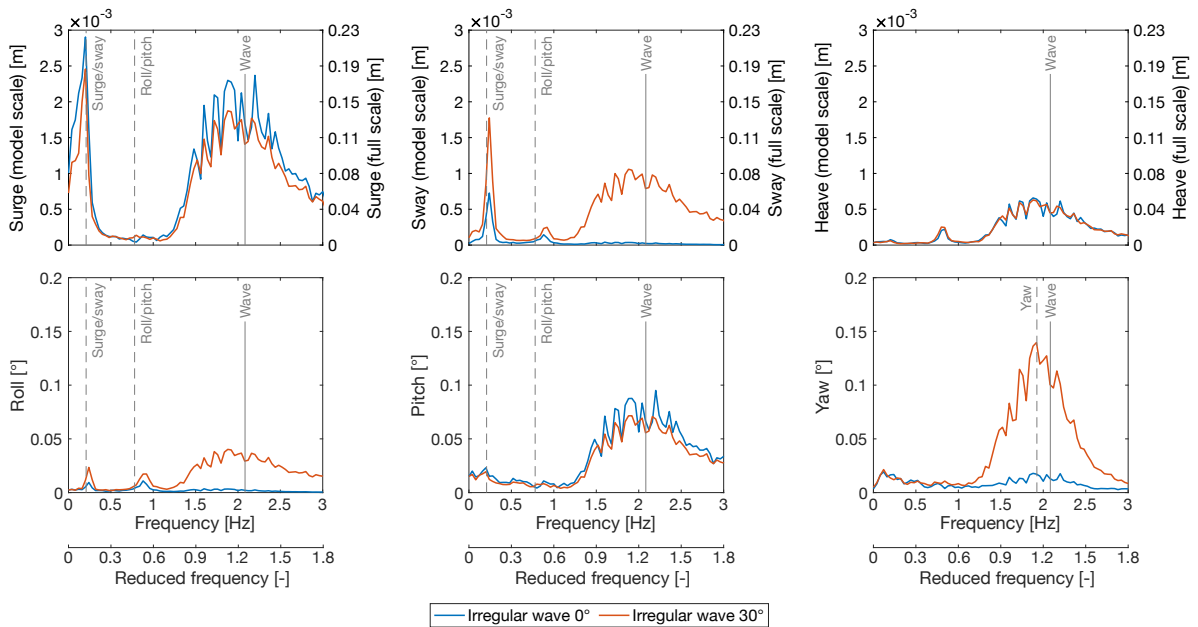


**Figure 3.** Spectra of wave-induced motions of the SOFTWIND 10 MW floating wind turbine subjected to irregular waves with a significant height of 5 m and a peak period of 12 s (full scale).



### 3 Results

The experimental campaign produced an extensive dataset (Fontanella et al., 2025). This paper examines a selected subset of cases, chosen for their scientific relevance and the insight they provide into the effects of turbine motion and wind farm layout.

The analysis of the results uses the aerodynamic thrust force ( $F_x$ ) and the torque ( $M_x$ ) as key indicators of rotor performance. Thrust plays a critical role in the coupled dynamics of floating wind turbines, linking aerodynamic forces to platform motion and contributing significantly to tower and blade loading. Torque, on the other hand, governs power generation and influences drivetrain dynamics. In the experiment, the wind turbines operated at a fixed rotor speed, so the aerodynamic power was directly calculated as the product of aerodynamic torque and rotor speed.

To enable comparison with other studies, rotor loads are also expressed in terms of non-dimensional coefficients. The thrust coefficient is defined as

$$C_t = \frac{F_x}{\frac{1}{2}\rho\pi R^2 U^2}, \quad (5)$$

and the torque coefficient as

$$C_q = \frac{M_x}{\frac{1}{2}\rho\pi R^3 U^2}. \quad (6)$$

#### 3.1 Time-average loads

This section presents an analysis of the average loads on the two wind turbines. Specifically, thrust and torque were evaluated in the fixed-tower base configuration to assess the aerodynamic response of each turbine and the overall wind farm behavior across different layouts (Sect. 3.1.1). The time-average power output was examined under prescribed motions of the upstream turbine to quantify the impact of platform motion on wake recovery (Sect. 3.1.2).

##### 3.1.1 Fixed tower base

The loads of WT1 in the fixed-tower base condition were measured in 40 repeated test runs. These repetitions were carried out throughout the experimental campaign, particularly after any changes in the test setup and following system initialization, for example at the beginning of each testing day, to ensure consistency of the measurements. The average thrust force was 36.17 N and the average torque was 2.87 Nm. The loads were consistent during the experimental campaign with maximum deviations from their mean values of  $\pm 0.33$  N for thrust and  $\pm 0.1$  Nm for torque. To verify the aerodynamic equivalence of WT2 with respect to WT1, WT2 was mounted on the robotic platform in WT1 position, and its performance was compared under identical operating conditions. The measured thrust force (35.9 N) and torque (3.03 Nm) for WT2 fell within the range recorded for WT1, confirming that WT2 rotor had equivalent aerodynamic performance.

The average WT2 loads are shown in Fig 4. When WT2 operated in free-stream conditions at the 5D position (with WT1 removed) and a wind speed of  $3.9 \text{ ms}^{-1}$ , its loads were consistent with those measured when the turbine was mounted on the robotic platform. At a wind speed of  $2.4 \text{ ms}^{-1}$ , which is representative of the average velocity in full-wake conditions, the thrust force of WT2 matched the scaled thrust of the DTU 10 MW turbine used as the reference in rotor design. These results

confirm that the wind tunnel provided a uniform inflow across the wind farm region and that the aerodynamic response of the downstream turbine was not significantly influenced by proximity to the end of the test section.

WT2 loads in farm scenarios with fixed WT1 were recorded across all farm configurations, with 2 to 9 repeated tests. In the configurations with aligned turbines and those with a lateral offset of  $1R$  the  $U_{RE}$  for WT2 is below the rated wind speed and the loads follow adequately the values of the DTU 10 MW at model scale.

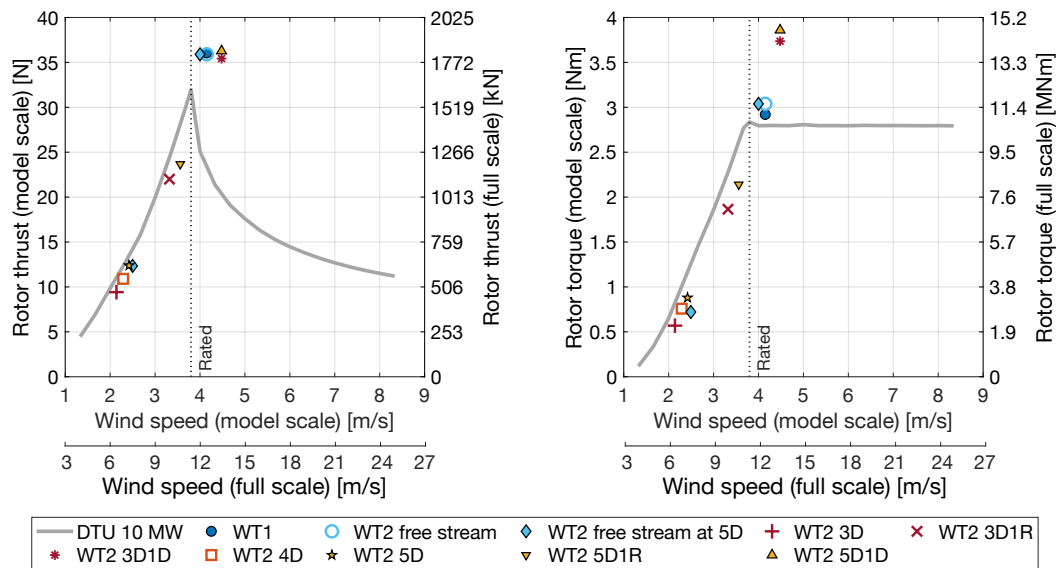


**Figure 4.** Rotor thrust and rotor torque of the two wind turbines in the scenario without platform motion and for different positions of WT2 with respect to WT1. The loads of WT1 and of WT2 in the free stream condition are plotted against the wind speed measured by the pitot system, while the loads of WT2 in all other configurations are plotted against the estimated rotor-effective wind speed.

In configurations with a lateral offset of  $1D$ , the effective wind speed  $U_{RE}$  for WT2 exceeds the rated wind speed, resulting in a tip-speed ratio lower than the optimal value for the rotor. While the thrust remains aligned with the free-stream condition, as intended when defining the operating parameters, the torque is higher.

### 295 3.1.2 Impact of platform motion on energy recovery

Large rotor motions induced by platform dynamics introduce unsteady variations in aerodynamic loads, which in turn alter the wake dynamics. This disturbance might enhance the natural mixing between the wake and the surrounding free stream, leading to earlier wake recovery compared to a case where the turbine is fixed at the tower base. Earlier mixing implies that the flow regains free-stream characteristics closer to the rotor, thereby increasing the available energy for a downstream turbine.

300 Wake velocity measurements taken at the WT2 positions shown only minor increases in mean wind speed relative to the fixed case (Fontanella et al., 2024). Larger improvements were observed in tests involving crosswind and yaw motions compared to purely along-wind motions, with more significant gains occurring at a distance of  $5D$ . The highest velocity increase was



recorded at  $5D$  in the case with yaw motion of  $2^\circ$  amplitude and a reduced frequency of 0.6, resulting in a 5% improvement over the fixed-bottom case. Under these conditions, the average wake velocity increased from  $2.5 \text{ ms}^{-1}$  to  $2.63 \text{ ms}^{-1}$ . Assuming constant power coefficient for a downstream turbine operating at these wind speeds, this velocity increase corresponds to a 16% gain in power output.

To directly assess the impact of motion of the upstream rotor on energy recovery, we measured the power output of WT2 placed at various positions in the wake of WT1. Figure 5 shows the ratio of WT2 power to WT1 power for various WT1 motion conditions, including the fixed-tower base reference case. For sinusoidal platform motions, the reported values represent the maximum WT2 power observed across all tested combinations of frequency and amplitude for each motion type.

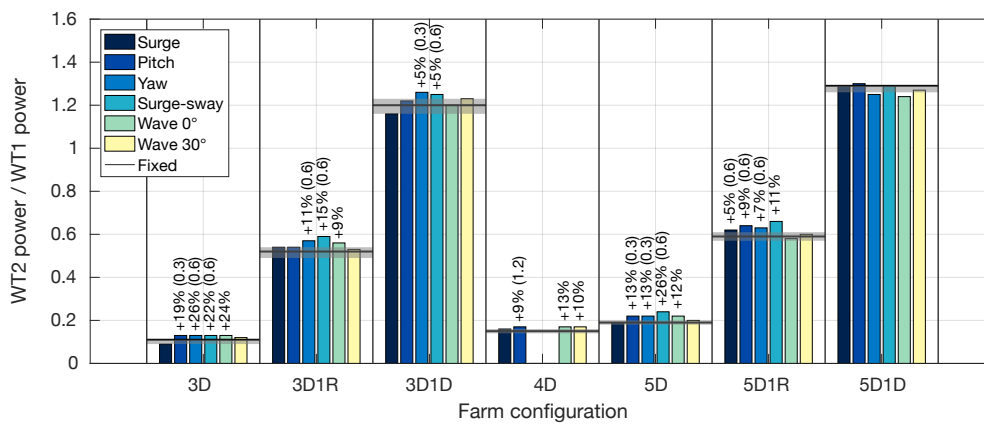


**Figure 5.** Maximum time-averaged power output of WT2, normalized by that of WT1, for various motion scenarios of WT1. The shaded area shows WT2 power variability in fixed conditions. Percentages above the bars indicate improvements over the fixed case when they exceed this variability; values in parentheses denote the reduced frequencies of the sinusoidal motions at which these gains were observed.

When WT2 is fully aligned with WT1, it operates in the core of the wake and generates the lowest power. In the fixed case, WT2 power increases modestly from 11% to 18% of WT1 power as the distance between the turbines increases from  $3D$  to  $5D$ , reflecting gradual wake recovery. As expected, the power generated by WT2 improves with lateral offset from the wake centerline. At an offset of  $1R$ , WT2 produces approximately 55% of WT1 power. When the offset reaches  $1D$ , WT2 actually generates more power than WT1, consistent with the overspeed observed in the estimates of rotor-averaged wind speed.

When WT1 undergoes platform motion, WT2 power increases under certain motion types relative to the fixed case. The most significant power gains were observed with sinusoidal yaw and surge–sway motions at reduced frequencies of 0.3 and 0.6. Wake velocity measurements reported by Fontanella et al. (2024) indicate that these motion types have the strongest impact on wake recovery. Motions driven by stochastic wave excitation at  $0^\circ$  incidence led to power gains comparable to those observed under sinusoidal pitch motion. For instance, in the  $3D$  configuration, sinusoidal pitch motion resulted in a 26% increase in WT2 power, while wave-induced motion at  $0^\circ$ , which excited platform pitch, produced a similar gain of 24%. In contrast, wave excitation at  $30^\circ$  incidence, which introduced significant crosswind and yaw motions, did not consistently lead



to increased power output for WT2. This differs from the sinusoidal motion cases, where crosswind and yaw motions were generally associated with noticeable power gains.

325 While relative power gains are most pronounced when WT2 is fully aligned with WT1, they remain small in absolute terms due to the inherently low baseline power in this configuration. The highest relative power increases over the fixed-turbine case (+26%) were observed in two scenarios: the 3D aligned configuration with WT1 undergoing yaw motion ( $2^\circ$  amplitude, reduced frequency 0.3), and the 5D aligned configuration with WT1 undergoing sway motion of 0.032 m amplitude (2.4 m at full scale), perpendicular to the wind, with reduced frequency 0.3. In the 3D yaw case, WT2 power increased from 11% to 330 13% of WT1 power, corresponding to a rise from 7.7 W (1.17 MW at full scale) to 9.7 W (1.47 MW), while WT1 maintained a constant output of 72 W (10.93 MW). In the 5D sway case, WT2 power increased from 19% to 24% of WT1 power, rising from 13.8 W (2.1 MW at full scale) to 17.4 W (2.64 MW). These power increases are of the same order of magnitude as those estimated from wake velocity measurements along a crosswind line at hub height, as reported by Fontanella et al. (2024).

While relative gains are most pronounced in aligned configurations, the absolute power increases are more substantial in 335 partially misaligned layouts. For instance, in the 3D1R configuration, when WT1 underwent surge–sway motion at a reduced frequency of 0.6 with an amplitude of 0.032 m (equivalent to 2.4 m at full scale) and oriented at a  $45^\circ$  angle to the wind, the power output of WT2 increased from 52% to 59% of WT1 power. In absolute terms, this corresponds to a rise from 37.1 W (5.63 MW at full scale) to 42.5 W (6.45 MW at full scale). Conversely, when WT2 was laterally offset by a full rotor diameter (1D), the influence of WT1 motion on downstream power became negligible.

### 340 3.2 Dynamic loads from upstream turbine movement

In addition to promoting wake mixing, the disturbances introduced by rotor motions can propagate downstream and induce dynamic loading on other turbines in the wind farm.

Figure 6 shows the aerodynamic thrust and torque measured on WT1 and WT2 when WT1 undergoes surge and pitch motions at a reduced frequency of 0.6; in these tests, the two turbines are aligned and spaced 3D apart. In the figure, the load 345 time series were binned and phase-averaged according to WT1 platform motion to show variations at the platform motion frequency.

Surge and pitch motions are considered because both involve nacelle translation in the wind direction, directly altering the apparent wind speed at the rotor. In both cases, the thrust force on WT1 exhibits a clear sinusoidal variation at the same frequency as the platform motion. The peak thrust occurs at half the motion period, corresponding to the moment when the 350 nacelle is moving upstream at its maximum velocity. This behavior, well-documented in previous experimental and numerical studies (Bergua et al., 2023), confirms that thrust oscillations are primarily driven by variations in apparent wind due to platform motion.

WT2 also exhibits periodic fluctuations in thrust and torque, with the same frequency as the motion of WT1. However, the amplitude of these variations is significantly lower, and the peaks occur with a delay of approximately 0.4 times the platform 355 motion period relative to those of WT1. This time lag reflects the transport of flow disturbances generated by the upstream rotor: coherent flow structures induced by WT1 motion are advected through the wake and eventually interact with WT2,

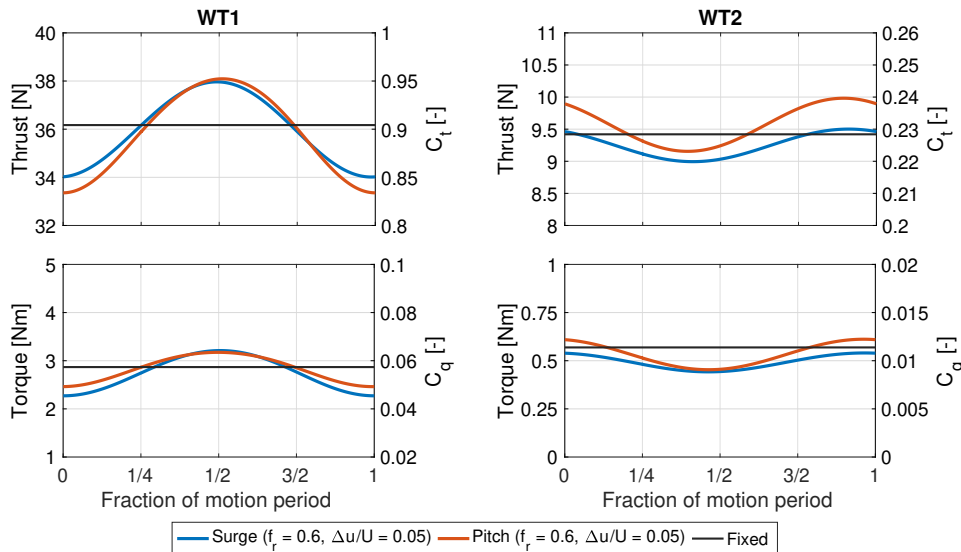


**Figure 6.** Rotor thrust and torque of WT1 and WT2 with WT1 undergoing surge and pitch motions at a reduced frequency ( $f_r$ ) of 0.6 and with apparent wind-to-undisturbed wind speed ratios ( $\Delta u/U$ ) of 5%, and with WT1 fixed.

generating the observed dynamic loading. The reduced amplitude of WT2 load oscillations, compared to WT1, is attributed to the diminished magnitude of wind speed fluctuations in the wake relative to the apparent wind speed variations experienced by WT1.

360 Figure 7 presents the Fast Fourier Transform (FFT) of the thrust force of WT2 when aligned with WT1 and positioned at various downstream distances. In these tests, WT1 undergoes surge or pitch motions at reduced frequencies of 0.3, 0.6, and 1.2. The FFT is utilized to determine whether the motion of the upstream rotor can introduce disturbances into the wake generating load harmonics on the downstream turbine at different frequencies than the motion frequency.

The load spectra of WT2 consistently show a sharp peak at the frequency of WT1 platform motion, corresponding to the  
 365 periodic load oscillations observed in Fig. 6. Across all tested configurations, this spectral peak is clearly visible at the excitation frequency, while the rest of the spectrum remains largely unchanged relative to the fixed case. Figures 6 and 7 show that surge and pitch motions producing equal variations in apparent wind speed lead to dynamic loads of comparable amplitude on the downstream wind turbine. In general, load variations are slightly higher for pitch motion than for surge motion.

WT2 exhibits a clear dynamic response at the frequency of WT1 motion when the reduced frequency is 0.3 or 0.6, confirming  
 370 that the upstream rotor motion is the primary driver of its load oscillations. This response is not observed at  $f_r = 1.2$ , indicating that higher-frequency motions of the upstream platform do not significantly influence the downstream turbine. This observation is consistent with the findings of Fontanella et al. (2024), who reported that wake velocity oscillations induced by platform motion diminish as the reduced frequency increases from 0.6 to 1.2. At a reduced frequency of 1.2, coherent flow structures generated by platform motion are weaker and dissipate closer to the rotor, limiting their persistence downstream.

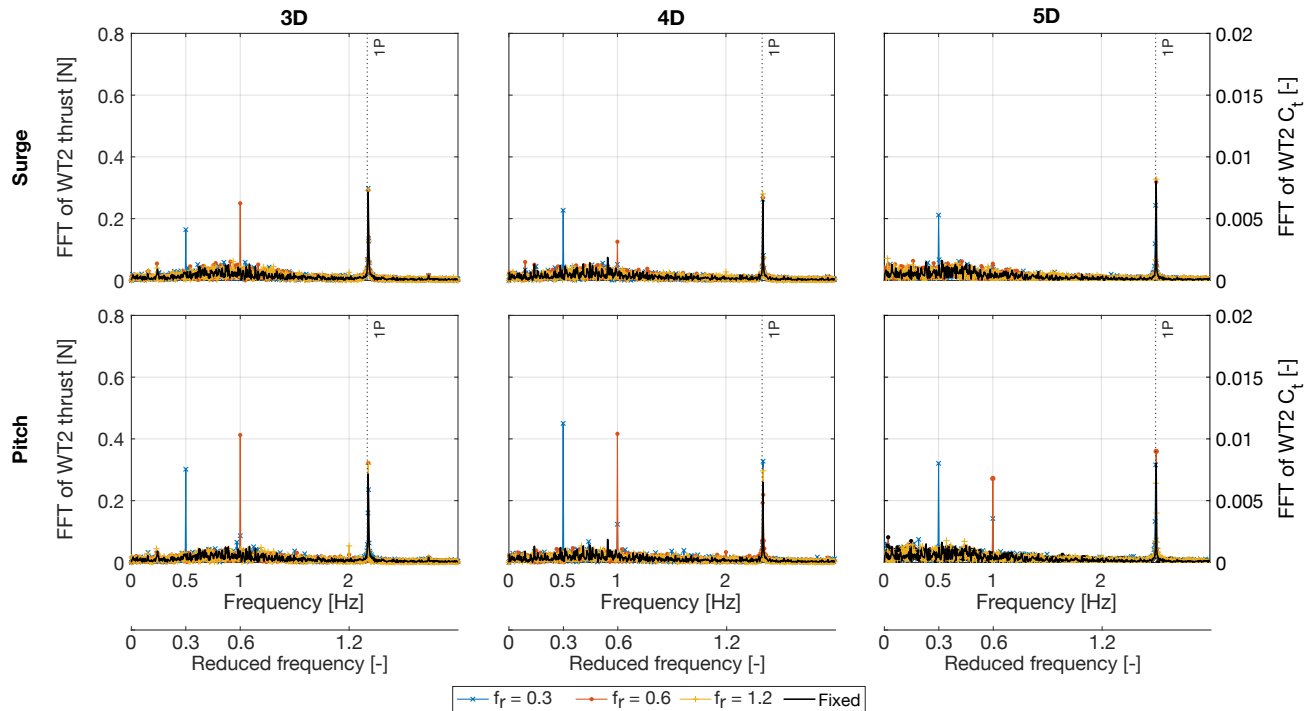


**Figure 7.** Fast Fourier Transform (FFT) of the thrust force on a downstream wind turbine operating in the wake of an upstream turbine subjected to sinusoidal surge and pitch motions. The turbines are aligned, and the downstream turbine is placed at multiple distances downstream of the upstream rotor.

375 At a reduced frequency of 0.6, the spectral peak in WT2 thrust is visible at distances of  $3D$  and  $4D$  from WT1 but disappears at  $5D$ . This again agrees with previous wake measurements of Fontanella et al. (2024), which showed that at larger distances, turbulence in the flow masks the periodic structures introduced by platform motion.

Interestingly, when WT1 is subjected to pitch motion at a reduced frequency of 0.3, a secondary spectral peak appears at twice the excitation frequency. The amplitude of this second harmonic increases with the spacing between the turbines.  
 380 This secondary peak does not appear under surge motion at the same reduced frequency, despite producing similar variations in apparent wind speed. The difference is attributed to the nature of pitch motion, which causes the rotor to tilt periodically upward and downward, vertically deflecting the wake. As a result, the wake undergoes oscillatory vertical motion. The observed second harmonic in WT2 load spectrum likely originates from this vertical wake movement: each time the wake shifts upward or downward, it induces a drop in thrust on WT2, generating a load fluctuation at twice the pitch motion frequency.

### 385 3.2.1 Effect of turbine relative positioning

The influence of lateral offset between the two turbines on the dynamic loading induced by the wake of a moving upstream rotor is examined for a pitch motion with an amplitude of  $1.3^\circ$  and a reduced frequency of 0.6. This case was selected because



the motion produces pronounced velocity oscillations in the wake of the upstream turbine and induces clear dynamic loads on the rotor of the downstream turbine in aligned configurations.

390 Figure 8 presents the power spectral density (PSD) of the wake velocity at hub height generated by this motion at different downstream locations, along with the amplitude of thrust and torque oscillations at the platform motion frequency experienced by the downstream turbine. In the figure, the thrust and torque amplitudes for the "Fixed" case represent the load oscillations experienced by WT2 when WT1 has fixed tower base. These values are extracted from the load spectra evaluated at a reduced frequency of 0.6. The observed oscillations in this configuration result from turbulence generated by the upstream turbine and the natural meandering of its wake.

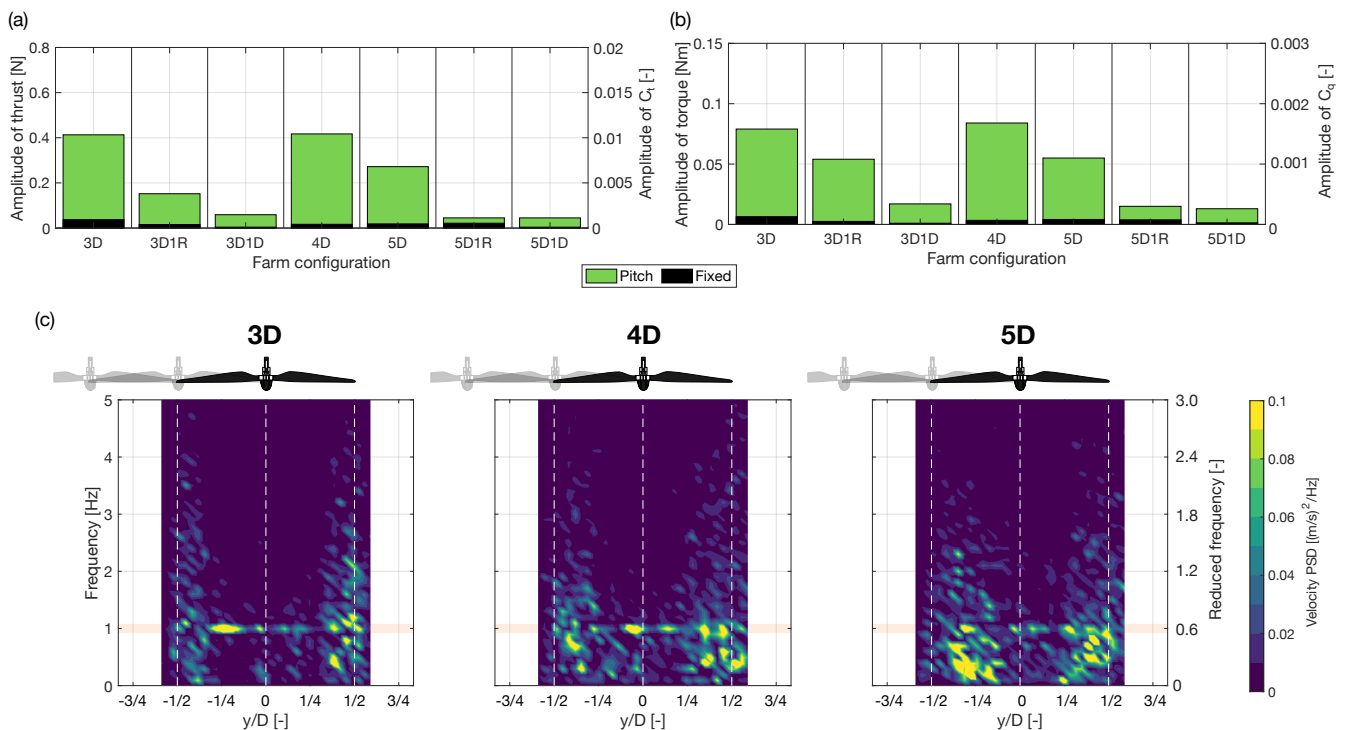


**Figure 8.** Effect of velocity oscillations induced by platform pitch motion on the loads of a downstream wind turbine operating in the wake, at varying downstream distances and crosswind positions. (a): amplitude of thrust oscillations on the downstream turbine at a reduced frequency of 0.6. (b): amplitude of torque oscillations on the downstream turbine. (c): power spectral density (PSD) of the velocity in the wake of the upstream turbine at different downstream locations.

395

In all farm configurations, WT2 experiences greater load amplitudes when WT1 is subject to platform motion than when it is fixed. The dynamic loads on WT2 reach their maximum when it is aligned with WT1. In this configuration, WT2 operates fully within the wake of WT1, and velocity fluctuations at the platform motion frequency affect the entire rotor-swept area. In the velocity PSD, the spectral peak corresponding to the motion frequency is less prominent at 5D than at closer distances, as it is masked by turbulence that increases downstream the rotor. As a result, the motion-induced loads on WT2 are also

400



reduced at  $5D$ , consistent with observations from Fig. 7. In the 4D configuration, the loads amplitude is maximum. This trend is consistent for both thrust and torque. The motion of WT1 induces zero-to-peak variations in WT2 thrust of 0.4 N (equivalent to 20.3 kN at full scale) representing approximately 3% of the average thrust developed by the turbine. Similarly, the torque variation reaches 0.084 Nm (319.3 kNm at full scale), corresponding to about 12% of the turbine average torque.

405 As WT2 is laterally offset from WT1, the amplitude of its dynamic load oscillations decreases. This reduction occurs because a larger portion of WT2 rotor operates outside the wake. With increasing offset, only part of the rotor is exposed to the unsteady wake flow, while the remainder encounters relatively steady free-stream conditions. The steadier inflow on part of the rotor mitigates the effects of the wake-induced fluctuations, leading to a net reduction in dynamic loading. When the offset reaches one rotor diameter, motion-induced loads on WT2 become negligible.

### 410 3.2.2 Effect of motion-driven wake meandering

While surge and pitch motions primarily induce oscillations in thrust that lead to a pulsating wake, motions in the crosswind (sway) and yaw directions predominantly excite lateral meandering of the wake (Fontanella et al., 2024). This side-to-side displacement introduces a different type of unsteadiness in the flow compared to the pulsing associated with surge and pitch. A rotor operating in such a wake is therefore subjected to dynamic loads that differ from those generated by along-wind motion of the upstream turbine. Section 3.2.3 investigates yaw motion, while Sect. 3.2.4 analyzes crosswind motion related to surge–sway movement.

### 3.2.3 Yaw motion

Figure 9 investigates the impact of sinusoidal yaw motion with a reduced frequency of 0.6 and an amplitude of  $2^\circ$  on the wake at a downstream distance of  $3D$ , and on the loads of WT2 placed in different positions relative to WT1 (loads were not measured in the 4D configuration).

425 Phase-averaged velocity time series at hub height show a coherent lateral displacement of the wake. This is particularly evident at the wake center, which deviates from the rotor axis and returns to it over the course of one motion period. This behavior is linked to the periodic change in rotor orientation relative to the wind, which causes the wake to be deflected laterally. In addition, the wake exhibits velocity variations that are out of phase on opposite sides. At any given moment, one side of the wake shows a velocity minimum while the other side exhibits a maximum. This alternating pattern is strongly correlated across the wake width and remains synchronized with the platform yaw motion. It reflects the effect of dynamic yaw, which creates an apparent wind speed with opposite signs on either side of the rotor.

When WT2 is aligned with WT1, in the 3D and 5D farm configurations, the sides of its rotor disk are exposed to opposing velocity variations: one side experiences a slight increase and the other a decrease. As a result, the effects tend to balance out, leading to minimal net load oscillations comparable to those caused by inflow turbulence experienced by the turbine when WT1 has a fixed tower base. However, when WT2 is laterally offset, by  $1R$  or  $1D$ , the symmetry is broken: a portion of the rotor disk is exposed to the unsteady wake, while the rest operates in relatively undisturbed flow. This asymmetric inflow causes pronounced variations in aerodynamic loading. In the 1R configuration, about half of the rotor is immersed in the

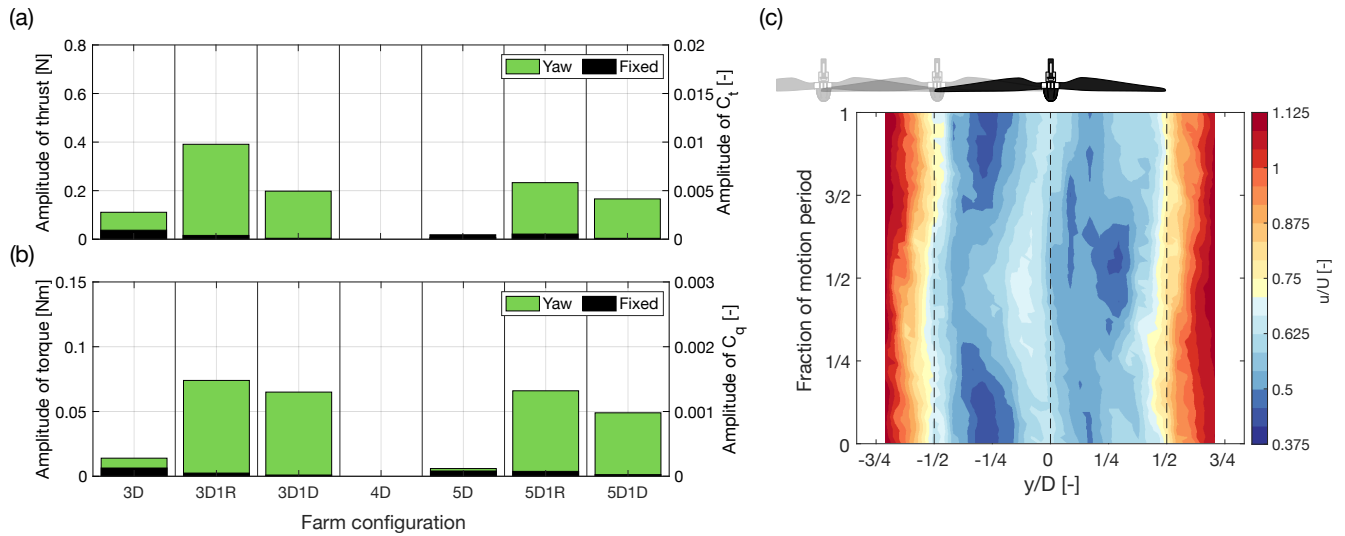


**Figure 9.** Effect of wake meandering induced by platform yaw motion with  $2^\circ$  amplitude and a reduced frequency 0.6 on the loads of a downstream wind turbine operating in the wake, at varying downstream distances and crosswind positions. (a): amplitude of thrust oscillations on the downstream turbine. (b): amplitude of torque oscillations on the downstream turbine. (c): phase-averaged velocity in the wake of the upstream turbine caused by yaw motion at a downstream distance of 3 rotor diameters.

fluctuating wake, leading to substantial unbalanced loads. In the 1D case, only the outer portion of the rotor is affected by velocity oscillations, resulting in a smaller load response than in the 1R case. In the 3D1R configuration, WT2 experiences zero-to-peak thrust variations of 0.4 N (equivalent to 20.3 kN at full scale) and torque variations of 0.074 Nm (281.2 kNm at full scale). These values are comparable to the load fluctuations observed in the 3D aligned configuration when WT1 undergoes pitch motion with an amplitude of  $1.3^\circ$  and a reduced frequency of 0.6. This indicates that a downstream turbine can experience similar dynamic loading whether it is fully immersed in a pulsating wake induced by pitch motion or partially exposed to a laterally meandering wake caused by yaw motion.

### 3.2.4 Crosswind motion

Figure 10 illustrates the effect of sinusoidal surge–sway motion at various angles  $\gamma$  and with  $f_r = 0.6$  on the wake at a downstream distance of  $3D$ , as well as on the aerodynamic loads of WT2 placed at different positions relative to WT1 (loads were not measured for the 4D configuration). When  $\gamma = 0^\circ$ , the motion corresponds to pure surge, producing velocity oscillations concentrated in the center of the wake. As the motion angle increases, the wake exhibits more pronounced lateral meandering, similar to what is observed in yaw motion. This phenomenon is especially pronounced at  $\gamma = 90^\circ$ , where the peak in relative velocity at the center of the wake alternates between the two sides of the rotor.

In the farm configuration with aligned turbines at a distance of  $3D$ , the amplitude of WT2 load oscillations at the platform motion frequency decreases as the motion angle  $\gamma$  increases. This trend reflects a shift from wake pulsation to lateral meander-

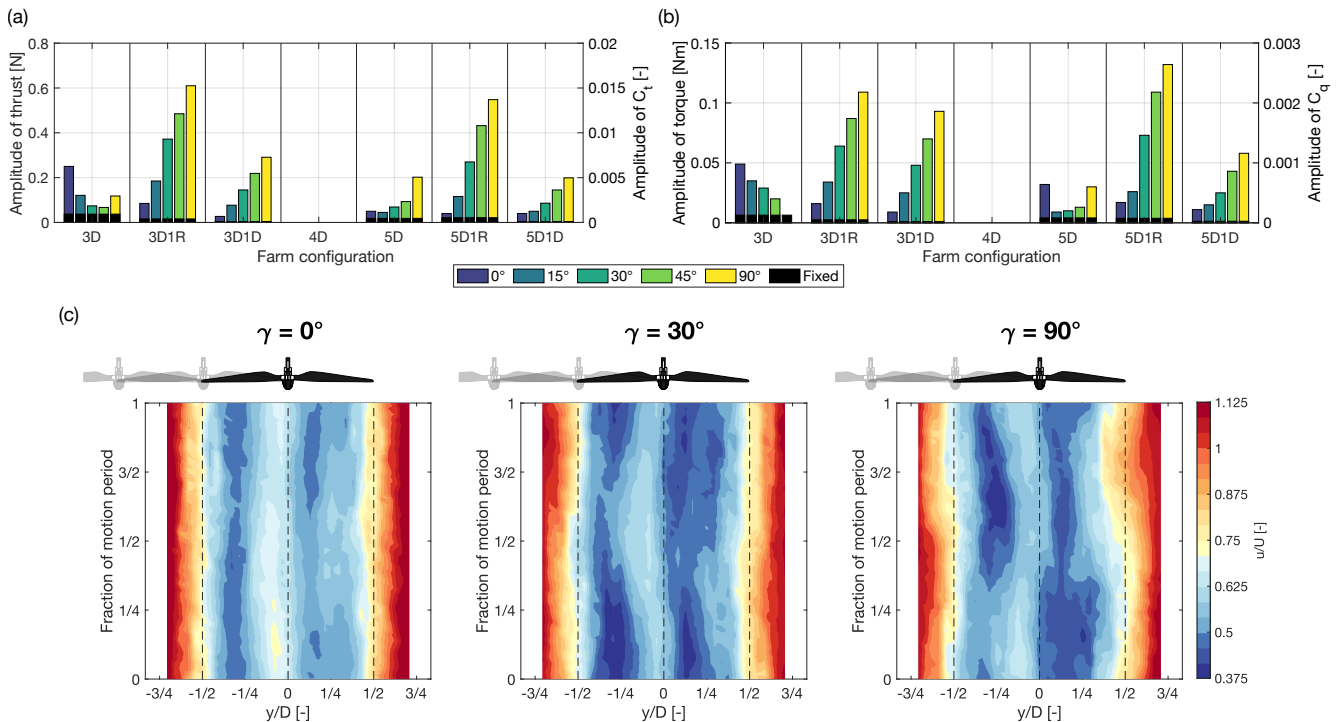


**Figure 10.** Effect of wake meandering induced by platform translational motion with reduced frequency 0.6 and various angles relative to the wind direction on the loads of a downstream wind turbine operating in the wake, at different downstream distances and crosswind positions. **(a):** amplitude of thrust oscillations on the downstream turbine. **(b):** amplitude of torque oscillations on the downstream turbine. **(c):** phase-averaged velocity in the wake of the upstream turbine at a downstream distance of 3 rotor diameters for a translational motion at different angles  $\gamma$  relative to the wind direction.

450 ing. As explained in the yaw motion case, meandering-induced velocity fluctuations tend to cancel out across the rotor when the turbines are aligned, reducing dynamic loading. At  $5D$  spacing, this behavior is less pronounced. The dynamic loads on WT2 remain nearly constant for motion angles up to  $45^\circ$  but show a noticeable increase at  $\gamma = 90^\circ$ . This rise in loading is likely due to pure sway motion which induces strong velocity oscillations in the wake that do not fully cancel out across the rotor.

455 In farm configurations where WT2 is laterally offset, the trend of loads reverses compared to aligned configurations. Here, the amplitude of dynamic loads increases with the motion angle, as only a portion of WT2 rotor is exposed to the periodic lateral wake meandering. As in the yaw motion case, the dynamic loads are higher in the 1R configurations than in the 1D configurations, reflecting the greater extent of rotor-wake interaction. In the 3D1R configuration, when WT1 undergoes motion at a  $30^\circ$  angle to the wind direction, WT2 experiences zero-to-peak thrust variations of 0.37 N (18.7 kN at full scale) and torque variations of 0.064 Nm (243.2 kNm at full scale). These values are similar to load fluctuations seen in the 3D aligned  
 460 configuration with pitch and yaw motions. The load amplitudes reach their maximum when WT1 motion is orthogonal to the



wind direction ( $\gamma = 90^\circ$ ), with thrust variations of 0.61 N (30.9 kN at full scale) and torque variations of 0.109 Nm (418.1 kNm at full scale).

### 3.2.5 Dynamic loads with irregular waves

465 Sinusoidal motion of the upstream wind turbine along individual directions produces distinct dynamic loads on a downstream turbine operating in its wake. In contrast, when WT1 undergoes wave-induced motion, it experiences simultaneous movements in all six degrees of freedom across a broad frequency range. The tests with wave-driven motions aim to assess whether the observations made under sinusoidal motion still hold in these more complex and realistic scenarios.

Figure 11 analyzes the effect of wave-driven motion on the thrust force spectrum of WT2, considering different wind farm configurations and wave headings of  $0^\circ$  and  $30^\circ$  relative to the wind direction.

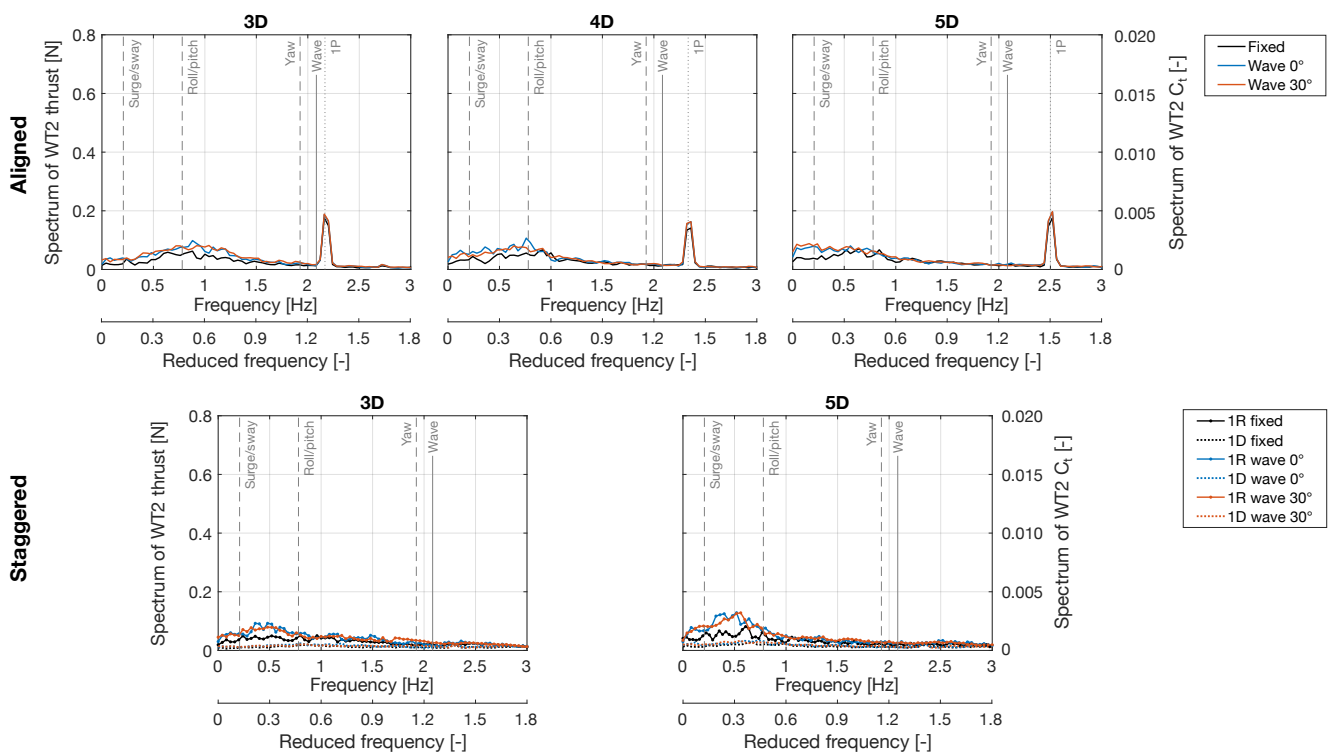


**Figure 11.** Spectrum of the thrust force on a downstream wind turbine operating at various positions in the wake of an upstream turbine subjected to wave-induced motions. The motions correspond to those of the SOFTWIND 10 MW floating wind turbine under irregular waves with a significant wave height of 5 m and a peak period of 12 s (full scale). The vertical dashed lines mark the natural frequencies of the upstream wind turbine rigid-body modes, the solid vertical line indicates the frequency associated with the peak wave period, and the dotted vertical line corresponds to the rotor rotation frequency of WT2 (1P).



In the cases with WT1 fixed, the thrust spectrum of WT2 is lowest when it is laterally offset by  $1D$  from WT1. The downstream turbine operates mostly outside the wake, experiencing minimal influence from upstream turbulence. In the aligned configuration and with a lateral offset of  $1R$ , the thrust spectrum is noticeably higher as wake interactions are stronger.

When WT1 was subjected to wave-induced motion, the thrust spectrum of WT2 increased at reduced frequencies below 475 0.6 in both the aligned and  $1R$  configurations. This indicates that upstream platform motions occurring near the surge/sway and roll/pitch natural frequencies contribute to dynamic loading of the downstream turbine in these layouts. The increase was similar for both wave headings ( $0^\circ$  and  $30^\circ$ ), suggesting limited directional sensitivity under the tested conditions.

Across all farm configurations, no increase in load amplitude was observed at frequencies near the spectral peak of the irregular waves (corresponding to a reduced frequency of approximately 1.25), despite the significant amplitude of platform 480 motions occurring at this frequency (see Fig. 3). This result aligns with previous sinusoidal motion tests, which demonstrated that motions at reduced frequencies around 1.2 do not lead to appreciable load oscillations on the downstream turbine.

To facilitate comparison with sinusoidal cases, the amplitude of the WT2 thrust spectrum in the irregular wave case was evaluated at a reduced frequency of 0.6 for the 3D configuration. With upstream motion driven by  $0^\circ$  waves, which excite primarily surge and pitch motions, the thrust spectral amplitude increased from 0.05 N (2.5 kN at full scale) in the fixed-WT1 485 case to 0.08 N (4.1 kN at full scale) under wave-induced motion. However, this remains substantially lower than the dynamic loads induced by prescribed sinusoidal motion: WT2 experienced zero-to-peak thrust fluctuations of 0.25 N (12.7 kN at full scale) with sinusoidal surge at  $f_r = 0.6$ , and 0.4 N (20.3 kN at full scale) with sinusoidal pitch at the same frequency. These comparisons highlight the more moderate impact of wave-driven motion on the dynamic loading of a downstream turbine compared to idealized, high-amplitude sinusoidal excitations.

490 In cases with a lateral offset of  $1R$ , the increase in WT2 thrust spectrum relative to the fixed case was more pronounced than in the aligned cases, particularly at reduced frequencies below 0.5. At frequencies above 0.6, the spectrum remained nearly unchanged. In configurations with a  $1D$  lateral offset, the influence of wave-induced motion on WT2 thrust oscillations was minimal, confirming that the rotor was largely outside the region affected by the wake.

#### 4 Discussion

495 The analysis of aerodynamic loads from the two wind turbines was carried out from two complementary perspectives: the effect on average performance, particularly the power extracted by the downstream turbine, and the influence on dynamic loading, i.e., unsteady forces experienced by the downstream rotor.

In the low-turbulence, short-spacing conditions considered in the experiment (3-to-5 rotor diameters), large, low-frequency motions of the upstream rotor were found to modestly enhance the power extracted by the downstream turbine. These enhance- 500 ments were particularly pronounced when the upstream turbine underwent sinusoidal motions in yaw or crosswind directions. In one case, WT2 power increased by 26% over the fixed-turbine baseline, though this translated to only a 2 W (0.3 MW at full scale) increase in absolute terms. Similarly, in partially offset configurations, surge–sway motions led to power increases of up to 5.4 W (equivalent to 0.82 MW at full scale).



505 However, the power gains observed under idealized sinusoidal motion were only partially reproduced in tests involving realistic wave-driven platform responses of a 10 MW spar floating wind turbine. In particular, wave excitation aligned with the wind direction ( $0^\circ$  heading), which excited pitch motion, resulted in downstream power gains similar to those observed under prescribed sinusoidal pitch motion. In contrast, wave excitation at  $30^\circ$  incidence, which introduces combined crosswind and yaw motions, did not consistently lead to power increases in the downstream turbine. This differs from the sinusoidal motion tests, where motions in the yaw and crosswind directions were generally associated with improvements in wake recovery and power output. These results suggest that the irregularity, phase coupling, and lower coherence of real platform responses may limit the effectiveness of wake recovery mechanisms that appear more pronounced under idealized, single-degree-of-freedom sinusoidal motions.

515 Regarding dynamic loading, sinusoidal motion tests clearly showed that the frequencies of upstream turbine motion were directly reflected in the aerodynamic loads on the downstream rotor, with a well-defined periodic response. The magnitude of these dynamic loads depended on turbine distance, offset, and the type of motion of the upstream wind turbine. For instance, load fluctuations reached up to 12% of the mean torque and 3% of the mean thrust when WT2 operated fully within the wake of WT1, which was undergoing wind-aligned motion (surge or pitch), resulting in wake pulsation. Comparable load amplitudes were also observed when WT2 was only partially immersed in a laterally-meandering wake, generated by crosswind or yaw motions of WT1. Both wake pulsing and meandering can induce substantial cyclic loading; pulsing predominantly in fully aligned turbine configurations, and meandering when there is a lateral offset between the turbines. In real operating conditions, the first scenario is likely to occur when waves are aligned with the wind, exciting surge and pitch motions, and when wind is aligned to wind farm rows placing downwind turbines directly in the full wake of upstream machines. The second scenario may arise under significant wind-wave misalignment and when the wind approaches the wind farm at an angle, resulting in partial wake exposure for downstream turbines and increased wake meandering due to lateral or yaw-induced motion.

525 Irregular wave-induced motions reproduced these dynamics with broader spectral content and lower amplitude. The key behaviors, such as increased load oscillations for the downstream turbine at low frequencies, persisted although the absolute loading levels were smaller than in sinusoidal tests.

530 These results suggest a tradeoff: platform motions can promote modest energy gains downstream but also introduce additional cyclic loading. Whether this tradeoff remains in high-turbulence atmospheric conditions or with greater turbine spacing or with dynamic blade pitch and generator torque control remains an open question. In more realistic atmospheric conditions, turbulence is expected to become the dominant driver of wake behavior, including mixing, recovery, and meandering (Wu and Porté-Agel, 2012; Hodgson et al., 2023). Further research is needed to assess the validity of these conclusions when: the downstream turbine is located farther downstream; both turbines are in motion; and rotor inclination reduces effective swept area or deflects the wake vertically. These might be important factors not captured in the present experimental setup.



## 535 5 Conclusions

This study investigated, through wind tunnel experiments, how the motion of a floating wind turbine affects the performance and dynamic loading of a downstream turbine operating in its wake. The upstream turbine was subjected to controlled platform motions, both sinusoidal and wave-induced, while the downstream turbine remained fixed and was tested in different relative positions.

540 In low-turbulence conditions and short spacing (3–5 rotor diameters), large-amplitude, low-frequency motions of the upstream turbine, especially in yaw and crosswind directions, led to moderate increases in the power output of the downstream turbine. In the most favorable cases, power increased by up to 26% over the fixed case, although absolute gains remained limited. These gains were most evident in sinusoidal tests and only partially reflected in realistic wave-induced motion scenarios.

At the same time, upstream platform motion introduced periodic flow disturbances that propagated downstream and increased dynamic loading on the waked turbine. The magnitude and frequency content of these dynamic loads depended on the  
545 type of motion, relative turbine positioning, and turbine-to-turbine distance. Load oscillations reached up to 12% of the mean torque and 3% of the mean thrust in certain farm configurations, with wake pulsing induced by along-wind motions and lateral wake meandering driven by crosswind and yaw motions both contributing similarly to the cyclic loading of the downstream turbine.

550 Key patterns in the aerodynamic loads of the downstream wind turbine identified under sinusoidal motion were also evident in tests involving realistic wave-induced motion. However, the amplitudes of the resulting loads were lower, reflecting the broader frequency content of wave-driven platform response and its interaction with the turbine wake.

Overall, platform-induced wake dynamics can modestly enhance energy capture but also introduce increased cyclic loads. Sinusoidal motion tests are effective for isolating key wake mechanisms, while tests with wave-driven motions provide a  
555 realistic assessment of performance and loading.

Further studies are needed to assess whether the trends observed under controlled conditions persist under higher-turbulence inflows and when multiple turbines are in motion. However, these findings of this study clearly underline the importance of considering wake–motion coupling in the design and analysis of future floating wind farms.

*Data availability.* Measurements of the upstream wind turbine wake under various platform motions are available at <https://doi.org/10.5281/zenodo.13994980>. Load measurements for two wind turbines in various farm setups and motion conditions, including those not covered here, are available at <https://doi.org/10.5281/zenodo.15582187>.



*Author contributions.* All authors prepared and conducted the experiment, and analyzed the measurement data. AF wrote the first draft of the article, while all authors contributed to its review and editing. MB, and AB have procured the funding. MB, SM, and AB have supervised the work.

565 *Competing interests.* At least one of the (co-)authors is a member of the editorial board of Wind Energy Science.

*Acknowledgements.* This research has been funded by the European Union – NextGenerationEU, M4C2 I1.1, Progetto PRIN 2022 "NET-TUNO", Prot. 2022PFLPHS, CUP D53D23003930006.



## References

- Angelou, N., Mann, J., and Dubreuil-Boisclair, C.: Revealing inflow and wake conditions of a 6 MW floating turbine, *Wind Energy Science*, 8, 1511–1531, <https://doi.org/10.5194/wes-8-1511-2023>, 2023.
- Arabgolarcheh, A., Micallef, D., and Benini, E.: The impact of platform motion phase differences on the power and load performance of tandem floating offshore wind turbines, *Energy*, 284, 129 271, <https://doi.org/https://doi.org/10.1016/j.energy.2023.129271>, 2023.
- Arnal, V.: Experimental modelling of a floating wind turbine using a “software-in-the-loop” approach, Theses, École centrale de Nantes, <https://theses.hal.science/tel-03237441>, 2020.
- 575 Bak, C., Zahle, F., Bitsche, R., Kim, T., Yde, A., Henriksen, L. C., Hansen, M. H., Blasques, J. P. A. A., Gaunaa, M., and Natarajan, A.: The DTU 10-MW Reference Wind Turbine, danish Wind Power Research 2013; Conference date: 27-05-2013 Through 28-05-2013, 2013.
- Bayati, I., Belloli, M., Bernini, L., and Zasso, A.: Wind Tunnel Wake Measurements of Floating Offshore Wind Turbines, vol. 137, pp. 214–222, <https://doi.org/10.1016/j.egypro.2017.10.375>, 2017a.
- Bayati, I., Belloli, M., Bernini, L., and Zasso, A.: Aerodynamic design methodology for wind tunnel tests of wind turbine rotors, *Journal of*  
580 *Wind Engineering and Industrial Aerodynamics*, 167, 217 – 227, <https://doi.org/https://doi.org/10.1016/j.jweia.2017.05.004>, 2017b.
- Behrens de Luna, R., Perez-Becker, S., Saverin, J., Marten, D., Papi, F., Ducasse, M.-L., Bonnefoy, F., Bianchini, A., and Paschereit, C.-O.: Quantifying the impact of modeling fidelity on different substructure concepts for floating offshore wind turbines – Part 1: Validation of the hydrodynamic module QBlade-Ocean, *Wind Energy Science*, 9, 623–649, <https://doi.org/10.5194/wes-9-623-2024>, 2024.
- Bergua, R., Robertson, A., Jonkman, J., Branlard, E., Fontanella, A., Belloli, M., Schito, P., Zasso, A., Persico, G., Sanvito, A., Amet, E.,  
585 Brun, C., Campaña Alonso, G., Martín-San-Román, R., Cai, R., Cai, J., Qian, Q., Maoshi, W., Beardsell, A., Pirrung, G., Ramos-García, N., Shi, W., Fu, J., Corniglion, R., Lovera, A., Galván, J., Nygaard, T. A., dos Santos, C. R., Gilbert, P., Joulin, P.-A., Blondel, F., Frickel, E., Chen, P., Hu, Z., Boisard, R., Yilmazlar, K., Croce, A., Harnois, V., Zhang, L., Li, Y., Aristondo, A., Mendikoa Alonso, I., Mancini, S., Boorsma, K., Savenije, F., Marten, D., Soto-Valle, R., Schulz, C. W., Netzband, S., Bianchini, A., Papi, F., Cioni, S., Trubat, P., Alarcon, D., Molins, C., Cormier, M., Brüker, K., Lutz, T., Xiao, Q., Deng, Z., Haudin, F., and Goveas, A.: OC6 project Phase III: validation of  
590 the aerodynamic loading on a wind turbine rotor undergoing large motion caused by a floating support structure, *Wind Energy Science*, 8, 465–485, <https://doi.org/10.5194/wes-8-465-2023>, 2023.
- Bossuyt, J., Ferčák, O., Sadek, Z., Meneveau, C., Gayme, D. F., and Cal, R. B.: Floating wind farm experiments through scaling for wake characterization, power extraction, and turbine dynamics, *Phys. Rev. Fluids*, 8, 120 501, <https://doi.org/10.1103/PhysRevFluids.8.120501>, 2023.
- 595 Carmo, L., Jonkman, J., and Thedin, R.: Investigating the interactions between wakes and floating wind turbines using FAST.Farm, *Wind Energy Science*, 9, 1827–1847, <https://doi.org/10.5194/wes-9-1827-2024>, 2024.
- Chitteth Ramachandran, R., Desmond, C., Judge, F., Serraris, J.-J., and Murphy, J.: Floating wind turbines: marine operations challenges and opportunities, *Wind Energy Science*, 7, 903–924, <https://doi.org/10.5194/wes-7-903-2022>, 2022.
- Firpo, A., Sanvito, A. G., Persico, G., Dossena, V., Schito, P., and Zasso, A.: Multi-fidelity actuator-line modelling of FOWT wakes, *Journal*  
600 *of Physics: Conference Series*, 2767, 052 050, <https://doi.org/10.1088/1742-6596/2767/5/052050>, 2024.
- Fontanella, A., Bayati, I., Mikkelsen, R., Belloli, M., and Zasso, A.: UNAFLOW: a holistic wind tunnel experiment about the aerodynamic response of floating wind turbines under imposed surge motion, *Wind Energy Science*, 6, 1169–1190, <https://doi.org/10.5194/wes-6-1169-2021>, 2021.



- Fontanella, A., Facchinetti, A., Di Carlo, S., and Belloli, M.: Wind tunnel investigation of the aerodynamic response of two 15 MW floating  
605 wind turbines, *Wind Energy Science*, 7, 1711–1729, <https://doi.org/10.5194/wes-7-1711-2022>, 2022a.
- Fontanella, A., Zasso, A., and Belloli, M.: Wind tunnel investigation of the wake-flow response for a floating turbine subjected to surge  
motion, *Journal of Physics: Conference Series*, 2265, 042 023, <https://doi.org/10.1088/1742-6596/2265/4/042023>, 2022b.
- Fontanella, A., Fusetti, A., Cioni, S., Papi, F., Muggiasca, S., Persico, G., Dossena, V., Bianchini, A., and Belloli, M.: Wake Development in  
Floating Wind Turbines: New Insights and Open Dataset from Wind Tunnel Experiments, *Wind Energy Science Discussions*, 2024, 1–23,  
610 <https://doi.org/10.5194/wes-2024-140>, 2024.
- Fontanella, A., Cioni, S., Papi, F., Muggiasca, S., Bianchini, A., and Belloli, M.: NETTUNO Experiment 2 – Ef-  
fects of floating wind turbine motion on a downstream turbine performance and loads, <https://www.nettuno-project.it>,  
<https://doi.org/https://doi.org/10.5281/zenodo.15582187>, accessed: 05/06/2025, 2025.
- Gaertner, E., Rinker, J., Sethuraman, L., Zahle, F., Anderson, B., Barter, G., Abbas, N., Meng, F., Bortolotti, P., Skrzypinski, W., Scott, G.,  
615 Feil, R., Bredmose, H., Dykes, K., Shields, M., Allen, C., and Viselli, A.: Definition of the IEA 15-Megawatt Offshore Reference Wind  
Turbine, Tech. rep., International Energy Agency, <https://www.nrel.gov/docs/fy20osti/75698.pdf>, 2020.
- Hodgson, E. L., Madsen, M. H. A., and Andersen, S. J.: Effects of turbulent inflow time scales on wind turbine wake behavior and recovery,  
*Physics of Fluids*, 35, 095 125, <https://doi.org/10.1063/5.0162311>, 2023.
- Li, Y., Yu, W., and Sarlak, H.: Wake interaction of dual surging FOWT rotors in tandem, *Renewable Energy*, 239, 122 062,  
620 <https://doi.org/https://doi.org/10.1016/j.renene.2024.122062>, 2025.
- Messmer, T., Hölling, M., and Peinke, J.: Enhanced recovery caused by nonlinear dynamics in the wake of a floating offshore wind turbine,  
*Journal of Fluid Mechanics*, 984, A66, <https://doi.org/10.1017/jfm.2024.175>, 2024a.
- Messmer, T., Peinke, J., and Hölling, M.: Wind tunnel investigation on the recovery and dynamics of the wake of a floating offshore  
wind turbine subjected to low inflow turbulence, *Journal of Physics: Conference Series*, 2767, 092 083, [https://doi.org/10.1088/1742-  
625 6596/2767/9/092083](https://doi.org/10.1088/1742-6596/2767/9/092083), 2024b.
- Meyers, J., Bottasso, C., Dykes, K., Fleming, P., Gebraad, P., Giebel, G., Göçmen, T., and van Wingerden, J.-W.: Wind farm flow control:  
prospects and challenges, *Wind Energy Science*, 7, 2271–2306, <https://doi.org/10.5194/wes-7-2271-2022>, 2022.
- Micallef, D. and Rezaeiha, A.: Floating offshore wind turbine aerodynamics: Trends and future challenges, *Renewable and Sustainable  
Energy Reviews*, 152, 111 696, <https://doi.org/https://doi.org/10.1016/j.rser.2021.111696>, 2021.
- 630 Pagamonci, L., Papi, F., Cojocar, G., Belloli, M., and Bianchini, A.: How does turbulence affect wake development in floating wind turbines?  
A critical assessment, *Wind Energy Science Discussions*, 2025, 1–36, <https://doi.org/10.5194/wes-2024-169>, 2025.
- Papi, F., Troise, G., Behrens de Luna, R., Saverin, J., Perez-Becker, S., Marten, D., Ducasse, M.-L., and Bianchini, A.: Quantifying the  
impact of modeling fidelity on different substructure concepts – Part 2: Code-to-code comparison in realistic environmental conditions,  
*Wind Energy Science*, 9, 981–1004, <https://doi.org/10.5194/wes-9-981-2024>, 2024.
- 635 Ramos-García, N., González Horcas, S., Pegalajar-Jurado, A., Kontos, S., and Bredmose, H.: Investigation of the floating IEA wind 15-  
MW RWT using vortex methods Part II: Wake impact on downstream turbines under turbulent inflow, *Wind Energy*, 25, 1434–1463,  
<https://doi.org/https://doi.org/10.1002/we.2738>, 2022.
- Stevens, R. J. A. M., Hobbs, B. F., Ramos, A., and Meneveau, C.: Combining economic and fluid dynamic models to determine the optimal  
spacing in very large wind farms, *Wind Energy*, 20, 465–477, <https://doi.org/https://doi.org/10.1002/we.2016>, 2017.



- 640 Van Der Hoek, D., Ferreira, C. S., and Van Wingerden, J.-W.: Experimental comparison of induction control methods for wind farm power maximization on a scaled two-turbine setup, *Journal of Physics: Conference Series*, 2767, 092 064, <https://doi.org/10.1088/1742-6596/2767/9/092064>, <https://dx.doi.org/10.1088/1742-6596/2767/9/092064>, 2024.
- Van Der Hoek, D., Den Abbeele, B. V., Ferreira, C. S., and van Wingerden, J.-W.: Maximizing wind farm power output with the helix approach: Experimental validation and wake analysis using tomographic particle image velocimetry, *Wind Energy*, 27, 463–482, <https://doi.org/https://doi.org/10.1002/we.2896>, 2024.
- 645 Wu, Y.-T. and Porté-Agel, F.: Atmospheric Turbulence Effects on Wind-Turbine Wakes: An LES Study, *Energies*, 5, 5340–5362, <https://doi.org/10.3390/en5125340>, 2012.